Electron Backstreaming Determination for Ion Thrusters

Richard E. Wirz[1], Ira Katz[2], Dan M. Goebel[3], and John R. Anderson[4]
Jet Propulsion Laboratory, California Institute of Technology, Pasadena, CA, 91001

Electron backstreaming in ion thrusters is caused by the random flux of beam electrons past a potential barrier established by the accel grid. A technique that integrates this flux over the radial extent of the barrier reveals important aspects of electron backstreaming phenomena for individual beamlets, across the thruster beam, and throughout thruster life. For individual beamlets it was found that over 99% of the electron backstreaming occurs in a small annulus at the center of the beamlet that is less than 20% the area of the beamlet at the potential barrier established by the accel grid. For the thruster beam it was found that over 99% of the backstreaming current occurs inside of r = 6 cm for the over 28 cm diameter NSTAR grid. Initial validation against ELT data shows that the technique provides the correct behavior and magnitude of electron backstreaming limit, V_{ebs}. From the sensitivity analyses it is apparent that accel grid chamfering may be the dominant mechanism contributing to the sharp rise in $|V_{ebs}|$ observed in the ELT but does not explain the rise in ion transparency. Grid gap change also contributes to $|V_{ebs}|$ rise and large rises in ion transparency with thruster life for the center gridlet. Screen grid erosion contributes generally to rises in $|V_{ebs}|$ and ion transparency, but for the assumptions used herein, it appears to not have as much of an effect chamfering or grid gap change. Overall, it is apparent that accel grid chamfering, grid gap change, and screen grid erosion are important to the increase in electron backstreaming observed during the ELT.

Nomenclature

$\overline{c}$	=	average thermal speed
f_{ebs}	=	electron backstreaming fraction
I_{ebs}	=	electron backstreaming current
I_i	=	ion current
n_{bp}	=	average downstream beamlet plasma density
r	=	radius
T_e	=	electron temperature
V_{ebs}	=	electron backstreaming limit
ϕ	=	local potential
ϕ_{bp}	=	beam potential
ϕ_m	=	minimum potential along for a radial distance from beamlet axis
Γ_e	=	electron flux

I. Introduction

Electron backstreaming in ion thrusters is caused by beam electrons that flow back into the discharge chamber by exceeding the potential barrier established by the accel grid. A schematic of this potential barrier is shown in Figure 1, which shows approximate axial potential traces at differing radial positions in the beamlet. Excessive

[1] Senior Engineer, Electric Propulsion Group, 4800 Oak Grove, M-S 125-109. Richard.E.Wirz@jpl.nasa.gov
[2] Group Supervisor, Electric Propulsion Group, 4800 Oak Grove, M-S 125-109.
[3] Senior Research Scientist, Propulsion and Materials Engineering Section, 4800 Oak Grove, M-S 125-109.
[4] Senior Engineer, Electric Propulsion Group, 4800 Oak Grove, M-S 125-109.

electron backstreaming wastes valuable spacecraft power; therefore an electron backstreaming fraction, f_{ebs}, limit of 1% is typically used for ion thrusters [refer to equation (1) below]. The minimum accel grid voltage required to keep f_{ebs} below 1% is called the electron backstreaming limit, V_{ebs}. For this condition, the Deep Space One flight spare ion thruster used for the extended life test (ELT) lost the ability to run at full power (TH15) after processing 211 kg of xenon propellant due to an electron backstreaming limit that exceeded the capability of the accel grid power supply [1].

Electron backstreaming was first analyzed by Kaufman [2]. For grids sets with large screen to grid gaps compared to the accel grid hole diameter, and neglecting the beam space charge, he developed an analytical expression for the electron backstreaming limit, V_{ebs}, based on grid voltages and macroscopic grid dimensions. Nakano [3] later developed a method which assumes that thruster end-of-life (EOL) occurs when the "saddle point" voltage on the beamlet axis reaches 0 V. Williams, Goebel and Wilbur [4] used the concept of the axial saddle point to develop an analytical expression that predicts the electron backstreaming current for a single beamlet as a function of ion beamlet current, macroscopic grid dimensions, ion mass, and downstream electron temperature. This method, commonly referred to as the WGW method, accounts for many important contributors to electron backstreaming. Using inputs from multiple NSTAR thruster tests, the WGW model was used as part of a pre-launch investigation of the estimated life of the NSTAR thrusters currently being used the DAWN mission [1]. From this investigation it is apparent that the WGW model is a useful tool provided sufficient information about the thruster is known; however, it is very sensitive to the beamlet diameter and grid dimensions, and so provides only an estimate of the values.

As discussed below, electron backstreaming occurs over the entire beamlet and therefore a rigorous treatment that accounts for the radial variation of retarding potential and electron flux is required. The objective of this investigation is to present a new electron backstreaming model that uses knowledge of radial variation of potentials at the potential barrier and can be used for detailed and eroded grid geometries.

II. Technique and Formulation

Electron backstreaming is caused by the random flux of high energy electrons past the potential barrier established by the accel grid potential. The high energy electrons come from the tail of the thermal distribution of beam electrons. The retarding potential (the minimum potential measured along the direction of the beamlet axis) varies radially in the beamlet, resulting in a radial dependence of electron backstreaming within a given beamlet. The formulation below provides a technique that can be used with ion optics codes that compute the potential values for a beamlet. This technique also works with codes such as CEX2D-t which provide a detailed eroded geometry of the grids using time-dependent erosion as discussed in reference [5].

The backstreaming fraction, f_{ebs}, for a beamlet is the ratio of backstreaming electron current, I_{ebs}, to the outgoing ion current, I_i, through an individual gridlet or the entire grid surface, depending on the domain of the problem, such that

$$f_{ebs} \equiv \frac{I_{ebs}}{I_i} \tag{1}$$

Several ion optics codes calculate the ion current, I_i, for a single beamlet for given plasma and thruster operating conditions. These codes also compute the plasma potentials throughout the computational domain. With this information, the electron backstreaming for can be estimated by considering the electron momentum. In the beamlet region one can assume the electrons are nearly in thermal equilibrium; in addition the electron drift, inertial, magnetic, and frictional forces are negligible such that the electron density, n_e, at a local potential, ϕ, is described by Boltzmann's relation

$$n_e = n_{bp} \exp\left[\frac{\phi - \phi_{bp}}{T_e}\right] \tag{2}$$

where n_{bp}, is the average downstream beamlet density at the beam potential, ϕ_{bp}. For ion thrusters, the accel grid sets up a potential barrier in the beamlet to prevent prodigious backstreaming of beam electrons. The flux of backstreaming electrons from the beam across a local potential minimum, ϕ_m, that will make it back into the

discharge chamber can be determined by using the Boltzmann relation to determine the electron density at the location of a minimum potential as a function of the downstream beam plasma potential, ϕ_{bp}, and the beam plasma density, n_{bp}. Therefore, the one-sided thermal flux of electrons is

$$\Gamma_e = \frac{n_{bp}\overline{c}}{4}\exp\left[\frac{\phi_m - \phi_{bp}}{T_e}\right] \tag{3}$$

where $\overline{c}$ is the average thermal speed of the beam electrons at temperature T_e. The radial locus of local minimum potentials created by the accel grid typically resides nearly along upstream end of the accel grid. Therefore, the electron backstreaming flux can be considered radially dependent such that

$$\Gamma_e(r) = \frac{n_{bp}\overline{c}}{4}\exp\left[\frac{\phi_m(r) - \phi_{bp}}{T_e}\right] \tag{4}$$

The electron backstreaming current for a beamlet is then given by integrating over the beamlet along the local minimum potentials

$$I_{ebs} = e2\pi\int_0^{r_{\max}} \Gamma_e(r) r dr = e\left(\frac{n_{bp}\overline{c}}{4}\right)2\pi\int_0^{r_{\max}} \exp\left[\frac{\phi_m(r) - \phi_{bp}}{T_e}\right] r dr \tag{5}$$

where r_{max} is the minimum diameter of the accel grid aperture, and hence the maximum radius for electron backstreaming to the discharge chamber.

III. Results

The formulation from Section II is used in this section to examine the electron backstreaming for individual gridlets and across the beam of the NSTAR. These tools are also used to investigate the electron backstreaming behavior observed during the ELT.

A. Inputs and Gridlet Potential Solutions

Post-test analysis of the NSTAR thrusters at the conclusion of the LDT and ELT tests showed that the center region of the grids experienced the most erosion and accel grid aperture enlargement, features which lead to increased electron backstreaming and screen transparency [6, 1]. This worst-case erosion was simulated in reference [5] for the full duration of the ELT. In this investigation we utilize the results from these simulations, as discussed below, to provide the accel grid chamfer angles for sensitivity and validation efforts. The potential for the downstream beam plasma, ϕ_{bp}, and electron temperature, T_e, were taken as 15 V and 1.8 eV, respectively, as discussed in [1]. The upstream electron temperature used was 5 eV and the neutral densities for TH15 were taken as the average of the neutral from the exit plane neutral profiles in reference [7].

The nominal hot grid gap (during thruster operation) used for the center hole at BOL was the 0.30 mm spacing measured for TH15 in reference [8] (this assumes an initial cold grid gap of 0.66 mm and a lessening of the grid gap by 0.36 mm during thruster operation). Since data on the radial variation of the hot grid gap is unavailable, this study assumes that the hot grid gap varies linearly from 0.30 mm at the center grid to 0.66 mm at the grid periphery at BOL. Post-test analysis for the ELT showed that the cold grid gap had changed approximately -0.19 mm. Therefore, the EOL minimum hot grid gap was assumed to vary linearly from 0.11 mm at the center grid to 0.47 mm at the grid periphery at BOL. Sensitivity analyses given below show that reduction of hot grid gap on this order may help to explain sharp rises in the magnitude of the electron backstreaming at the end of life.

The potential fields for the beamlets are determined by CEX2D which is described in detail in reference [9]. To determine the electron backstreaming limit, V_{ebs}, for each case the accel grid voltage is swept through a range of voltage to find the point at which we achieve the backstreaming condition of f_{ebs} = 1% (similar to the method used to experimentally determine V_{ebs}) using the formulation from Section II.

B. EBS integration over single gridlets and thruster grid profiles

Electron backstreaming was determined for the NSTAR profiles shown in Figure 2, for which the beamlet currents were calculated from LDT and ELT Faraday probe traces using the technique discussed in reference [1]. Using these beamlet densities and the formulation from Section II, it was found that the potential barrier is essentially just upstream of the accel grid for most configurations. Integrating equation (5) over this potential barrier for several single beamlets it was found that over 99% of the electron backstreaming occurs in a small annulus that is less than 20% the size of the beamlet at this location. This concentration of electron backstreaming current can be seen from plots of the electron backstreaming current density versus beamlet radius, as shown in Figure 3. This plot is indicative of the electron backstreaming conditions in the beamlet for all conditions examined.

For the profiles in Figure 2 it is reasonable to use trapezoidal integration between radii 0, 2, 4, 6, 8, 10, and 13 to determine the backstreaming limit for the entire beam. Using this technique for ELT profiles at TH15 and TH9 the electron backstreaming limit was very near experimentally determined values as shown in Table 1. It was also found that over 99% of the backstreaming current occurs inside of r = 6 cm of the over 28 cm diameter NSTAR grids. For these profiles it was also found that $f_{ebs} \approx 10\%$ for the center hole when $f_{ebs} = 1\%$ for the entire beam. This correlation was used in the following analysis to perform sensitivities by examining the effects of erosion on the center hole taken from reference [5].

C. Electron backstreaming sensitivities and comparisons with ELT data

During test segments 4 and 6 of the ELT the NSTAR thruster was operated at full power (TH15) and the magnitude of the electron backstreaming limit rose dramatically (see Figure 7). Also, during these test segments the screen transparency to ions increased noticeably as shown in (see Figure 8). Before comparing to these observations it is important to understand the dependence of electron backstreaming on chamfering angle of the downstream end of the accel grid, grid spacing, and screen grid thickness. To facilitate the comparison with ELT data, the effect of these parameters on grid transparency to ions for the center hole will also be examined.

The erosion results for the center hole from reference [5] suggests that the chamfer angles of the accel grid grows from about 2° to 6° degrees during test segment 4, and from about 6° to 11.6° degrees during test segment 6. Examining the electron backstreaming limit, V_{ebs}, for these chamfer angles at grid spacings of 0.30, 0.20, and 0.11 mm (at a nominal end-of-life grid thickness of 0.32 mm and accel gridlet diameter of 1.410 mm) for the center hole shows a general increase in $|V_{ebs}|$ with increasing chamfer angle as shown in Figure 4. The grid transparency to ions was found to be constant for a given grid spacing regardless of chamfer angle (i.e., the grid transparency is 87.5 for l_g = 0.30 mm, 91.2 for l_g = 0.20 mm, and 93.2 for l_g = 0.11 mm). From these results it is apparent that increasing chamfer angle contributes to the change in backstreaming limit observed in the ELT but does not explain the rise in ion transparency.

If these results are plotted as a function of grid spacing (Figure 5), an increase in both transparency and $|V_{ebs}|$ is evident; however the change in V_{ebs} is not sufficiently steep to match the ELT results. This suggests that grid gap change and chamfering work together to increase the electron backstreaming limit. The transparency change is for the center hole only since the intermediate erosion estimates from reference [5] are only for the center hole.

To examine the effects of screen thickness we note that the erosion profiles do not include redeposition; therefore, the variation of screen grid thickness was simple taken to be proportional to the throughput, as done in reference [1]. Using this method, the screen grid thicknesses plotted in Figure 6 correspond to the test segments as shown on the top axis of the graph. The results for ion transparency and electron backstreaming limit in Figure 6 show that decreasing screen thickness generally causes both the magnitude of V_{ebs} and screen grid transparency to increase; however, the change in V_{ebs} is not nearly enough to explain the trends seen from the ELT (Figure 7).

Combining the effects of chamfering, grid spacing, and screen thickness yields the comparison with ELT data shown in Figure 7. The computated values assume the conditions for the beginning and end of Test Segments 4 and 6 for the center gridlet shown in Table 2. The trends in screen grid transparency from the computational results agree with the values shown in Figure 8; however, additional work is needed to correlate the screen grid transparency values for the center hole with the ELT data for the entire beam.

IV. Conclusions

The technique presented herein for calculating electron backstreaming reveals important aspects of electron backstreaming phenomenon for individual beamlets, across the thruster beam, and throughout thruster life. For individual beamlets it was found that over 99% of the electron backstreaming occurs in a small annulus at the center of the beamlet that is less than 20% the area of the beamlet at the potential barrier established by the accel grid. For

the thruster beam it was found that over 99% of the backstreaming current occurs inside of r = 6 cm for the over 28 cm diameter NSTAR grid.

Initial validation against ELT data shows that the technique provides the correct behavior and magnitude of electron backstreaming for the grid geometries and assumptions use herein. From the sensitivity analyses it is apparent that accel grid chamfering may be the dominant mechanism contributing to the sharp rise in $|V_{ebs}|$ observed in the ELT but does not explain the rise in ion transparency. Grid gap change also contributes to $|V_{ebs}|$ rise and large rises in ion transparency with thruster life. Screen grid erosion contributes generally to rises in $|V_{ebs}|$ and ion transparency, but for the assumptions used herein, it appears to not have as much of an effect as chamfering or grid gap change. Overall, it is apparent that accel grid chamfering, grid gap change, and screen grid erosion are important to the increase in electron backstreaming observed during the ELT. However, since many of the parameters used herein are uncertain it is important to perform additional validation and analysis of this technique and its sensitivity to the many inputs to this problem. For example, since this tool is intended to estimate thruster life it is important to rigorously propagate the error associated with the inputs to provide probabilistic failure analysis, similar to that performed in reference [1].

Appendix

Tables and Figures

Table 1. Calculated Electron Backstreaming Limit at ELT beginning-of-life.

EBS Limit	Measured	Calculated
TH15	**-150 V**	**-145 V**
TH9	**-130 V**	**-132 V**

Table 2. Assumed Center Hole Characteristics for the computational results shown in Figure 7.

Time	Chamfer Angle (°)	Grid Spacing (mm)	Screen Grid Thickness (mm)
Beginning of Test Segment 4	2.0	0.3	0.361
End of Test Segment 4	6.0	0.2	0.348
Beginning of Test Segment 6	2.0	0.2	0.344
End of Test Segment 6	6.0	0.11	0.333

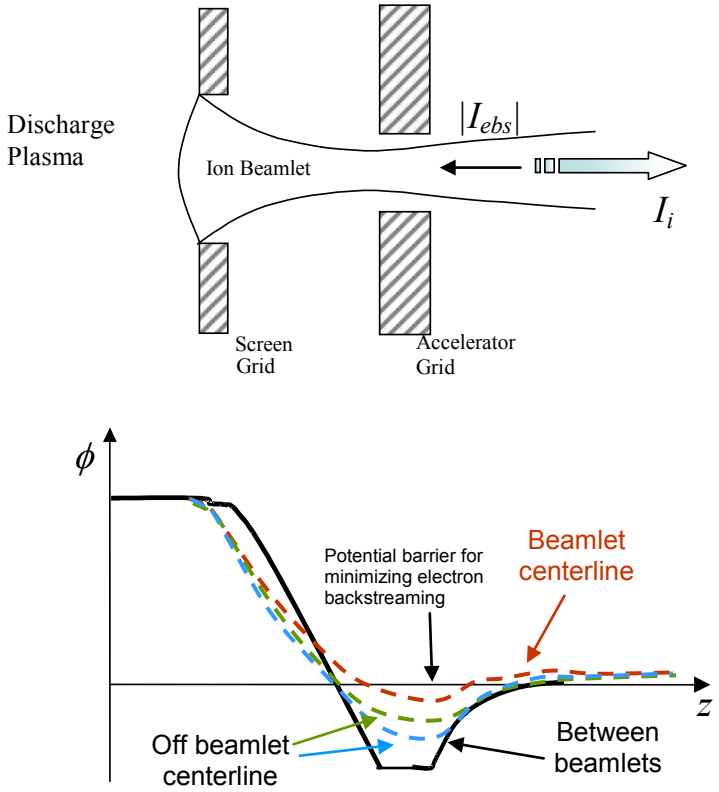

Figure 1. Schematic of beamlet showing approximate beamlet potentials at different radial positions from beamlet axis.

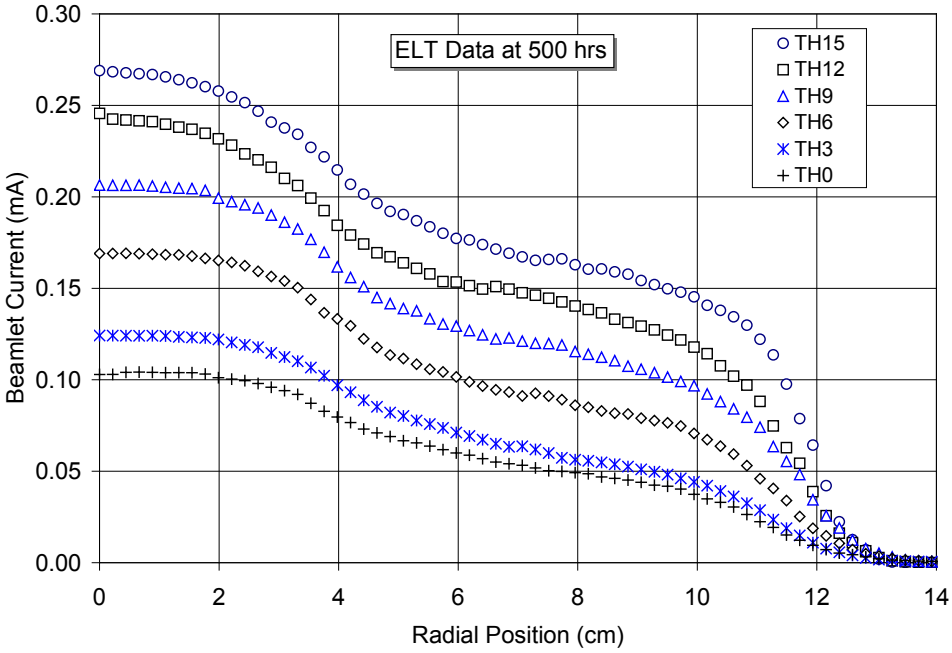

Figure 2. Beamlet current vs. radial position for LDT at TH15 and ELT for various throttle conditions.

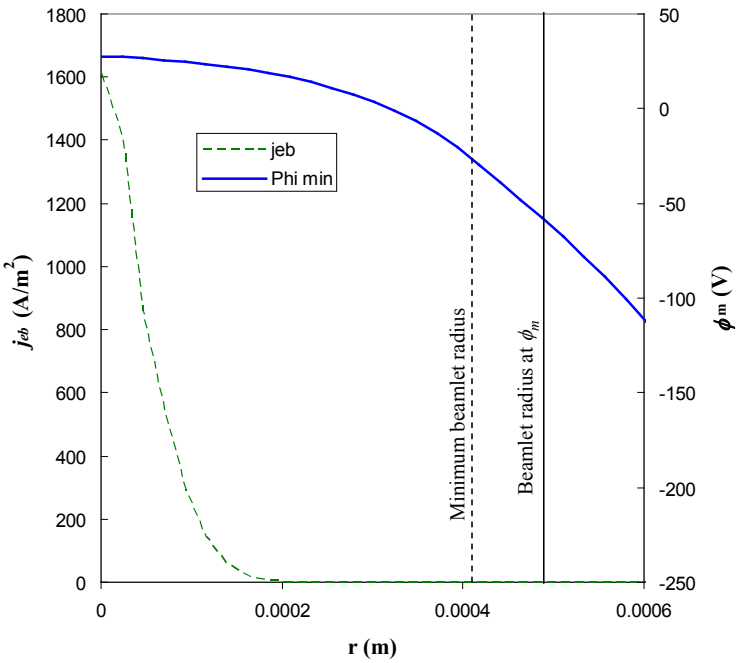

Figure 3. Electron backstreaming current density, j_{eb}, and minimum potential, ϕ_m, vs. beamlet radius for TH15 at ELT EOL condition for center beamlet. (Note: the minimum beamlet radius is typically found just upstream of the accel grid while the minimum potential is typically just downstream of the accel grid)

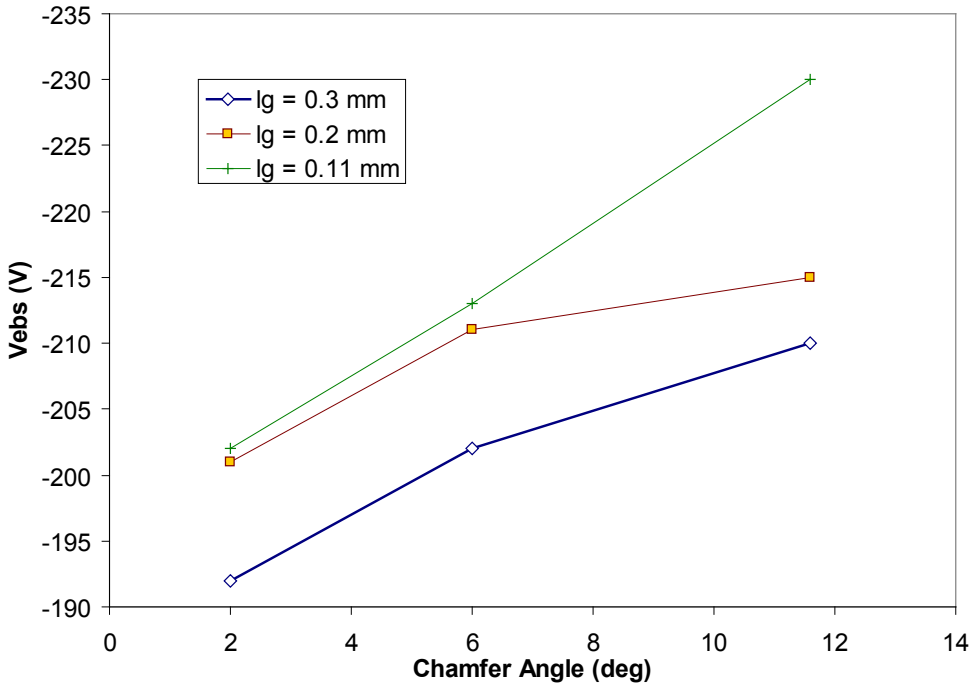

Figure 4. Electron Backstreaming Limit versus chamfer angle at grid gaps (lg) of 0.3, 0.2, and 0.11 mm.

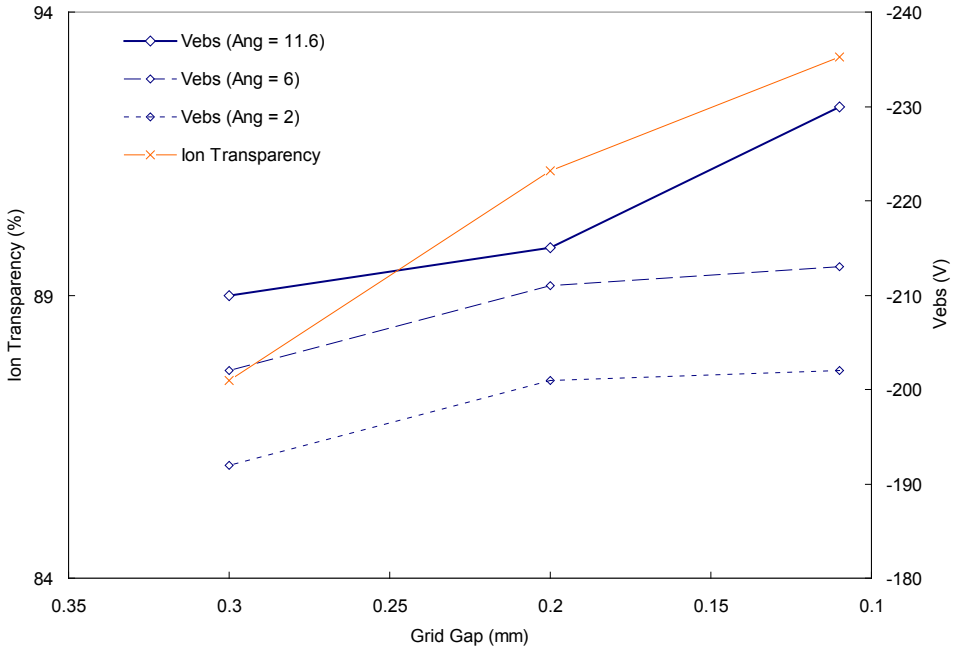

Figure 5. Electron Backstreaming Limit (Vebs) and Ion Transparency versus and grid gap for Chamfer Angles (Ang) of 2°, 6°, and 11.6°. (Note: transparency change is for center hole only)

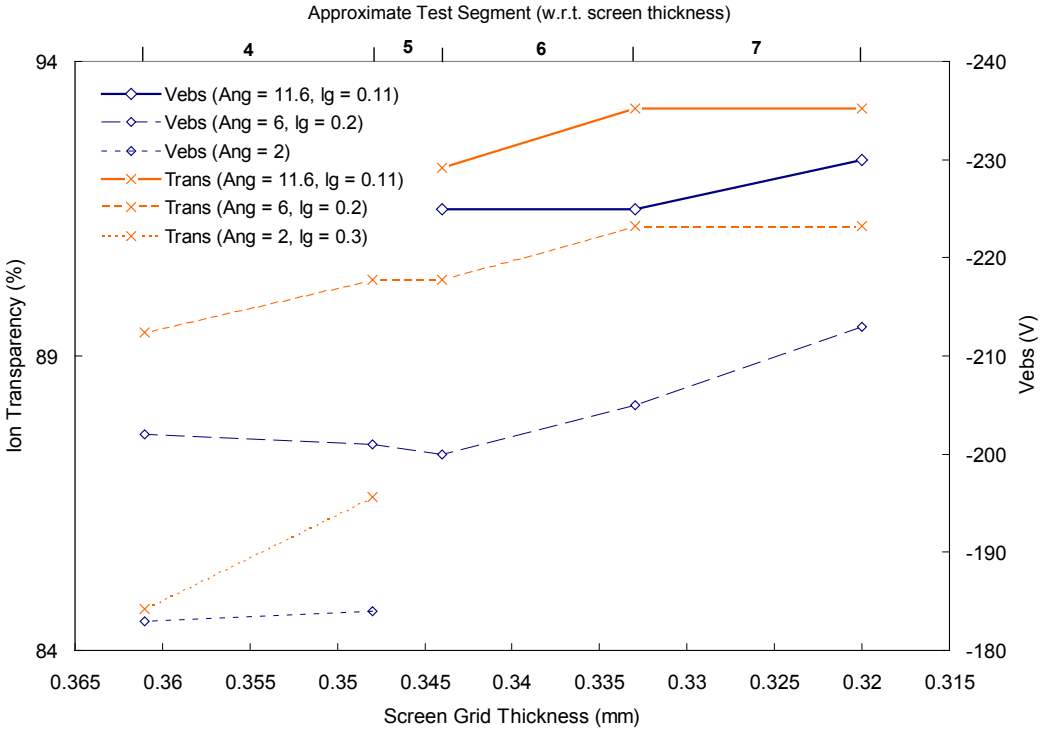

Figure 6. Electron Backstreaming Limit (Vebs) and Ion Transparency (Trans) variation with screen grid thickness for different combinations of chamfer angle (Ang) and grid spacing (lg). (Note: transparency change is for center hole only)

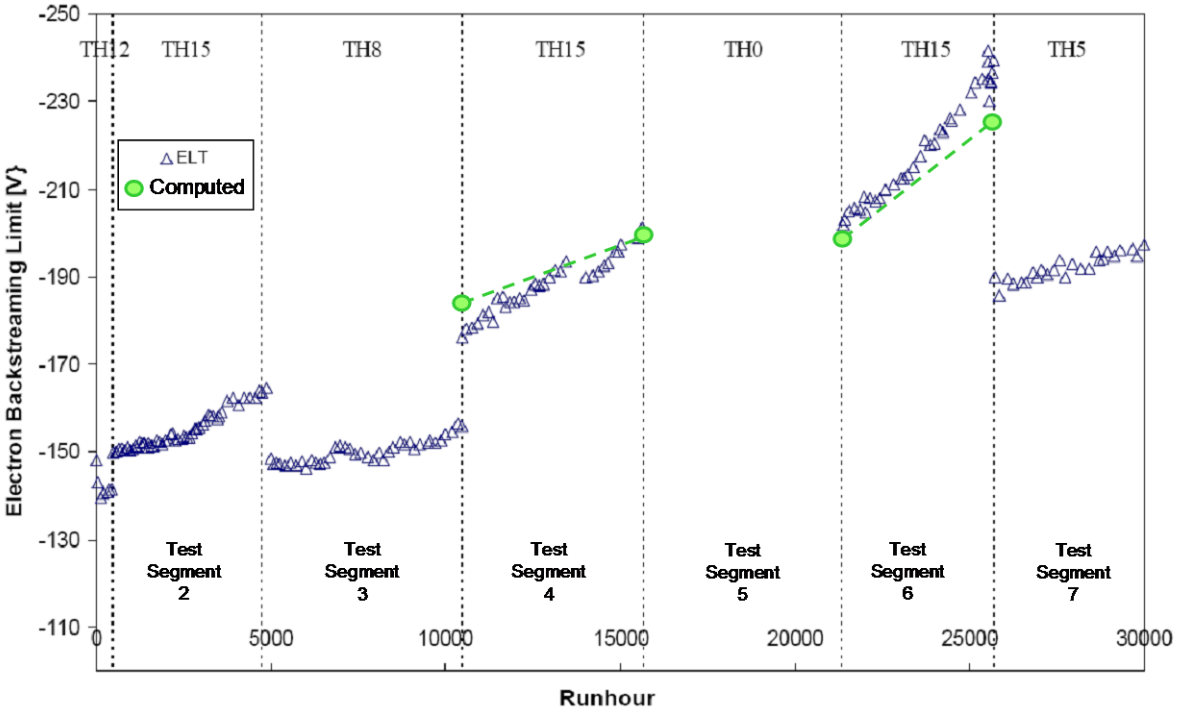

Figure 7. Electron Backstreaming Limit as a function of time for the ELT.

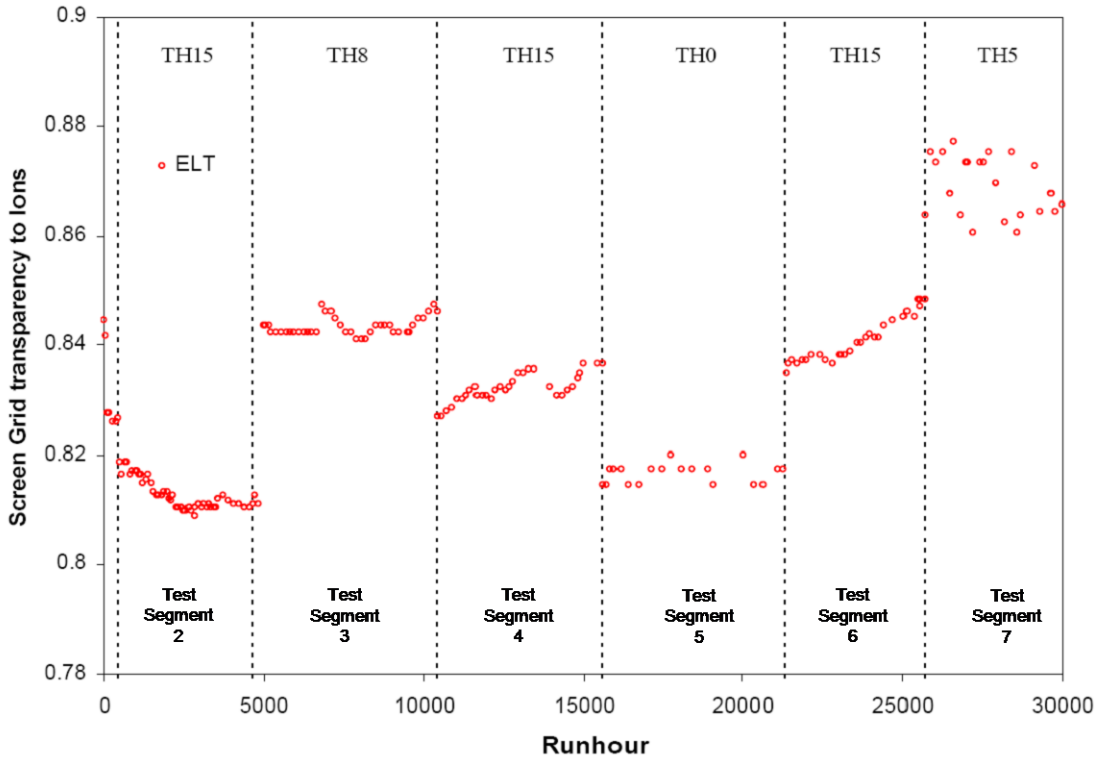

Figure 8. Screen grid transparency to ions as a function of time during the ELT.

Acknowledgments

The research described in this paper was carried out by the Jet Propulsion Laboratory, California Institute of Technology, under contract with the National Aeronautics and Space Administration.

References

[1] Brophy J. R., "Propellant Throughput Capability of the DAWN Ion Thrusters," IEPC-2007-279
[2] Kaufman H. R., "Technology of Electron-Bombardment Ion Thrusters," in *Advances in Electronics and Electron Physics*, Vol. 36, Ed. L. Marton, Academic Press, New York, 1974.
[3] Nakano M., "A Grid Lifetime Model for a 3-Grid Ion Engine," IEPC-01-84
[4] Williams J. D., Goebel D. M., Wilbur P. J., "Analytical Model of Electron Backstreaming for Ion Thrusters," AIAA-2003-4560
[5] Wirz R. E., Anderson J. R., Katz I., Goebel D. M., "Time Dependent Erosion of Ion Optics," AIAA-2008-4529
[6] Anderson J. R., et al, "Post-Test Analysis of the Deep Space One Spare Flight Thruster Ion Optics," AIAA 2004-3610
[7] Wirz R. E., "Discharge Plasma Processes of Ring-Cusp Ion Thrusters," Ph.D. Dissertation, Aeronautics, Caltech, Pasadena, CA, 2005, http://etd.caltech.edu/etd/available/etd-05232005-162628/.
[8] Diaz E. M., Soulas G. C., "Grid Gap Measurement for an NSTAR Ion Thruster," NASA/TM-2006-214249, IEPC-2005-244
[9] Brophy J. R., Katz I., Polk J., Anderson J. R., "Numerical Simulations of Ion Thruster Accelerator Grid Erosion," AIAA 2002-4261